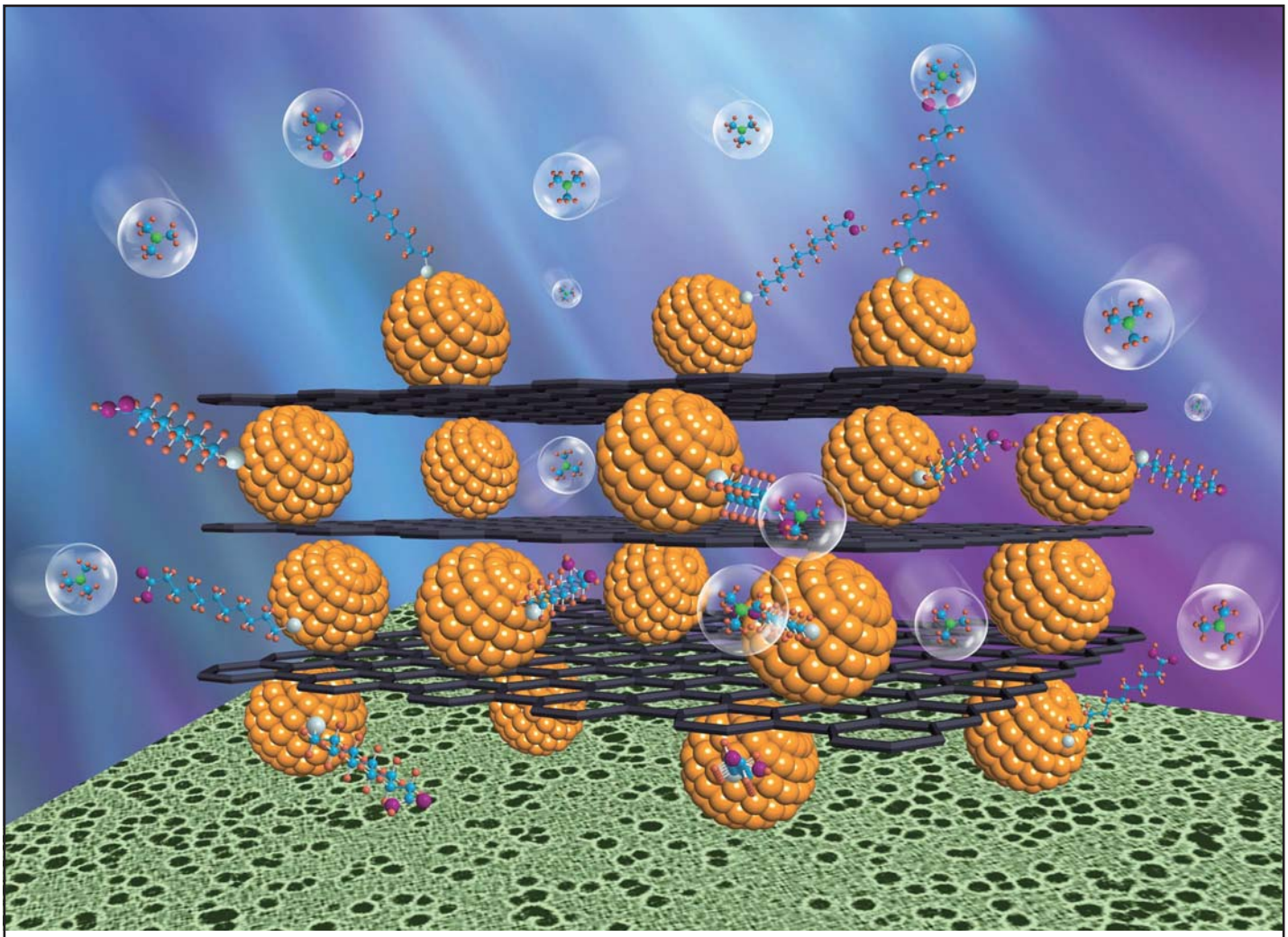

Highlighting work from the Xinxin Li group at State Key Laboratory of Transducer Technology, Shanghai Institute of Microsystem and Information Technology, Chinese Academy of Sciences, China.

Title: Porous-layered stack of functionalized AuNPs–rGO (gold nanoparticles–reduced graphene oxide) nanosheets as a sensing material for micro-gravimetric detection of chemical vapor

In oleylamine, gold nanoparticles (AuNPs) are grown *in situ* on graphene oxide (GO) sheets. The porous-stacked AuNPs–rGO nanostructure is formed by gas-phase reducing GO to rGO. This is loaded onto a resonant-cantilever for gravimetric sensing, resulting in high-resolution and high-selectivity detection of ppm-level trimethylamine vapor.

As featured in:

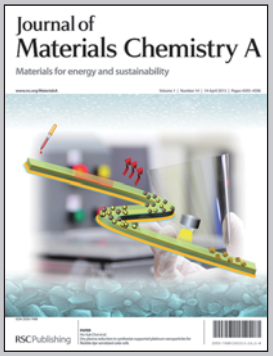

See Xinxin Li *et al.*, *J. Mater. Chem. A*, 2013, **1**, 4444.

RSC Publishing

www.rsc.org/MaterialsA

Registered Charity Number 207890

Journal of Materials Chemistry A

RSC Publishing

PAPER

Cite this: J. Mater. Chem. A, 2013, 1, 4444

Porous-layered stack of functionalized AuNP–rGO (gold nanoparticles–reduced graphene oxide) nanosheets as a sensing material for the micro-gravimetric detection of chemical vapor

Haitao Yu,[a] Pengcheng Xu,[a] D.-W. Lee[b] and Xinxin Li*[a]

Received 6th December 2012
Accepted 29th January 2013

DOI: 10.1039/c3ta01401k

www.rsc.org/MaterialsA

With oleylamine as a solvent and reducing agent, Au nanoparticles (AuNPs) are grown *in situ* on graphene oxide (GO) sheets. Thereafter, a porous-layered stack of AuNPs–GO nanosheets is formed by a gas-phase chemical reduction step. After the AuNPs are modified with 11-mercaptoundecanoic acid (11-MUA) to graft –COOH sensing groups to the amine, the functionalized AuNPs–rGO porous-layer stacked nanosheets are loaded onto a gravimetric resonant microcantilever for use as a mass sensing material. The rGO sheets serve as multi-layer nano-shelves to support and carry the functionalized AuNPs for gas adsorbing/sensing, while the AuNPs serve as nano-spacers between the rGO sheets to provide a high specific surface area for gas molecules accessing the material. The cantilever sensor experimentally exhibits a very rapid response to ppm-level trimethylamine (TMA) vapor, which is attributed to the novel sensing material. Compared with the hydrophilic AuNP–GO, the highly hydrophobic AuNP–rGO shows a much improved suppression to the noise from changes in environmental humidity. Featuring a rapid response, high sensitivity and good resistance to interference from environmental moisture, the novel sensing nanomaterial is promising in various chemical vapor detection applications.

Introduction

Nanoparticles and nanoparticle-based materials are attracting great interest due to their unique properties and potential in many applications. Gold nanoparticles (AuNPs) are of particular interest and are utilized in many fields such as chemistry, biology, catalysis, medicine and nanotechnology.[1–6] One of the important reasons is that AuNPs can be easily surface-modified by a self-assembled monolayer (SAM) to form functionalized AuNPs.[7–9] Therefore, AuNPs provide platform technologies for the functionalization of various chemical or biological ligands for the specific binding and detection of chemical molecules and biological targets.[10–12] The advantageous properties of AuNPs also allow researchers to develop novel bio/chemical sensors with improved sensitivity, stability and selectivity.[13]

With respect to chemical sensors utilising AuNPs, the sensing methods are mainly based on colorimetric,[14–16] fluorescence[17–19] and electrochemical[20,21] mechanisms, as described in the literature. Micro-gravimetric sensing techniques, *e.g.* adsorbed mass detection with a resonant microcantilever, have been considered as an ultra-sensitive tool for the on-the-spot detection of chemical vapors, microorganisms and DNA, due to its trace-level resolution, rapid response, tiny size and low-cost volume fabrication capability.[22–26] Incorporation of AuNPs into the cantilever-based sensing microsystems can further enhance both sensitivity, by their high surface area, and selectivity, by specific functionalization. Unfortunately, to the best knowledge of the authors, AuNPs have been seldom used in mass-type chemical sensors so far. This may be for two reasons. Firstly, the AuNPs tend to aggregate to form a condensed solid on their drying from solution, thereby dramatically decreasing the specific surface area. Secondly, a single layer or a thin film of the AuNP array cannot adsorb a sufficient quantity of gas-molecules (*i.e.* sufficient mass) for the micro-gravimetric sensor to generate a detectable sensing signal. According to the previous research reported by the US Pacific Northwest National Laboratory, when loaded with an organically functionalized AuNP film, the quartz crystal microbalance (QCM, a typical gravimetric sensor) was unable to generate an adequate sensing signal for the target molecules.[27,28] To retain the high surface area of AuNPs, it is crucial to keep the AuNPs in a monodispersed state after their drying from solution. Moreover, instead of a single-layer or thin-film structure, a multi-layered stack of AuNPs should be constructed onto the micro-gravimetric sensor to enhance the effective number of the sensing AuNPs. Laying dispersed AuNPs on the nano-shelves, just like putting books on library bookshelves, is expected to be a good solution.

[a]State Key Laboratory of Transducer Technology, Shanghai Institute of Microsystem and Information Technology, Chinese Academy of Sciences, Shanghai 200050, China. E-mail: xxli@mail.sim.ac.cn; Fax: +86-21-62513510; Tel: +86-21-62131794
[b]School of Mechanical Systems Engineering, Chonnam National University, Gwangju 500757, Korea

Graphene, a two-dimensional (2D) sheet of sp^2-hybridized carbon, has shown potential applications in nanometric electronic devices, sensors, biomedicines and mechanical resonators due to its unique electronic and mechanic properties.[29–33] Graphene and chemically derived graphene, such as graphene oxide (GO) and reduced graphene oxide (rGO), take on an extended honeycomb network structure which can be used as the basic building block of many three-dimensional nanostructures. In order to meet the two above-mentioned requirements for micro-gravimetric gas sensing, we herein propose a method to construct a porous-layered stack of functionalized AuNP–rGO nanosheets as a sensing material with a high effective specific surface area. As is schematically illustrated in Fig. 1, firstly AuNPs are grown *in situ* on the surface of GO sheets to form the AuNP–GO hybrid in oleylamine. The GO provides oxygen-containing groups which coordinate with Au ions and, aided by oleylamine, a reducing agent, the AuNPs are grown *via* a chemical reduction route. After oleylamine is removed, the porous-layer stacked nanostructure is formed, where the GO sheets are spaced by the AuNPs. Before the sensing-groups are modified on the AuNPs, the hydrophilic GO sheets are further reduced to hydrophobic rGO using a gas-phase reducing method. The AuNP–rGO is considered superior to AuNP–GO in terms of the elimination of environmental noise from humidity changes, as the hydrophilic GO easily adsorbs environmental moisture, which interferes with the sensing-signal. With 11-mercaptoundecanoic acid (11-MUA) grafted onto the AuNPs, the novel porous-layer stacked sensing material is loaded onto the designated micro-region of our lab-made resonant microcantilevers to form micro-gravimetric trimethylamine (TMA) sensors.[34] The sensors have experimentally exhibited a rapid response, high sensitivity and a satisfactory selectivity to ppm-level TMA vapor. The effect of reducing GO into rGO on depressing environmental moisture noise has also been verified experimentally.

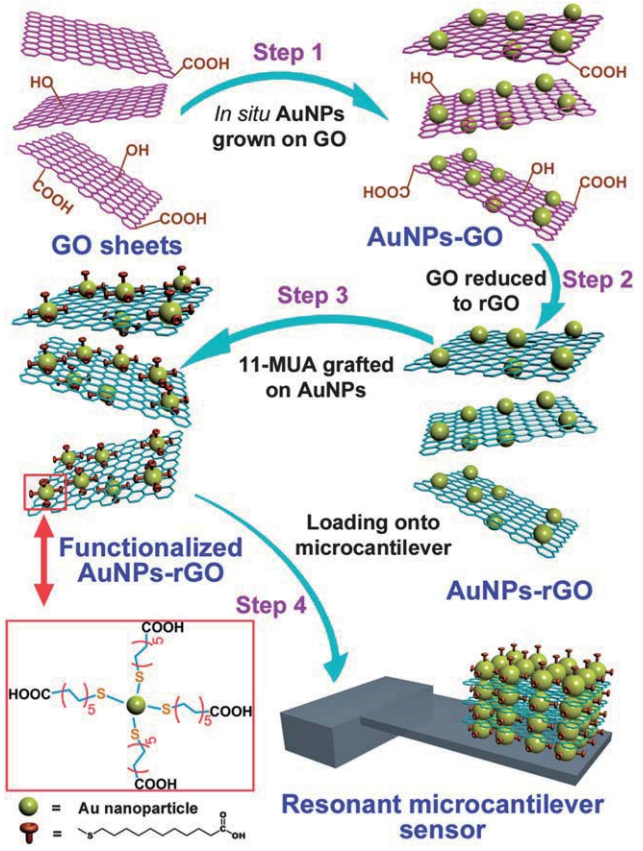

Fig. 1 Schematic route for preparing the functionalized AuNP–rGO and loading the sensing material onto a gravimetric microcantilever.

Experimental section

Chemicals

Graphite powder is purchased from Sinopharm Chemical Reagent Co., Ltd. $HAuCl_4 \cdot 4H_2O$ is purchased from Alfa Aesar. Oleylamine and 11-MUA are purchased from Sigma-Aldrich. Ethanol, *n*-hexane, formaldehyde, acetone, benzene, KNO_3, $KMnO_4$, 98 wt% H_2SO_4, 30 wt% H_2O_2, 37 wt% HCl and 68 wt% HNO_3 are of analytical grade and purchased from Shanghai Chemical Corporation. All of the gaseous chemicals are purchased from Dalian Special Gas Industry Company.

Preparation of GO

The GO sheets are firstly prepared by using a modified Hummers method.[35,36] The modified Hummers preparation process is detailed as follows. Under slow stirring, 1.2 g KNO_3 is added into 23 mL concentrated H_2SO_4 (98 wt%) to form a stable solution. At room temperature, 1.0 g graphite powder is added and stirred for 10 min. Then, 6.4 g $KMnO_4$ is slowly added into the mixture under vigorous stirring at 0 °C. The mixture is stirred for 2 h to form a dark green suspension. Then, 80 mL deionized water is added. The oxidization process is terminated by mixing in deionized water (100 mL) and 30 wt% H_2O_2 solution (6 mL). The produced graphite oxide is collected by centrifugation. Then, the graphite oxide is sequentially washed with 10 wt% HCl solution and deionized water, three times. After drying at 60 °C for 24 h, the graphite oxide product is redispersed in deionized water under ultrasonic vibration. The formed suspension has a concentration of about 2.5 mg mL^{-1}. The suspension is centrifuged at 2000 rpm for 10 min to remove the small amount of non-exfoliated micro-particle residue. In order to obtain GO paper, the homogeneous colloidal suspension is collected by filtration with a PTFE (polytetrafluoroethylene) membrane and drying in air at 60 °C. After brief treatment in liquid nitrogen (77 K), the GO paper is detached from the PTFE membrane.

Synthesis of AuNP–GO hybrid nanostructure

All of the glassware and magnetic stirrers for the experiments are washed with *agua regia* (37 wt% HCl–68 wt% HNO_3 = 3 : 1 in volume). **Caution!** *Agua regia* solution reacts violently with organic compounds and should be handled with extreme care. Typically, the GO film with an accurate mass of 37.5 mg is added to oleylamine (20 mL). In a 120 °C oil bath, vigorous stirring is implemented for 10 min. Then, 45.2 mg of $HAuCl_4 \cdot 4H_2O$ is quickly added and reacted for another 10 min. Thereafter, the temperature is increased to 180 °C. After refluxing for 10 min, the reaction is terminated. After being cooled to room

temperature, the dispersion is transferred into a centrifuge tube (with 50 mL volume) for high-speed centrifuging (rotating speed = 12 000 rpm) for 10 min. Then the sample is washed with *n*-hexane and ethanol. Finally, the sample is dried under vacuum.

Gas-phase chemical reduction to form AuNP–rGO sheets

Under gas purging with a mixed flow of Ar (285 SCCM) and H_2 (15 SCCM), the as-prepared AuNP–GO hybrid is treated in a 300 °C tube furnace for 2 h, until the oxygen-containing groups (–COOH/–OH/epoxy) in the AuNP–GO hybrid are chemically reduced, thereby transforming the hybrid into hydrophobic AuNP–rGO.

Functionalization of AuNP–rGO with the sensing group 11-MUA

–COOH groups are grafted onto the AuNPs by the self-assembly of 11-MUA, using a similar method which was detailed in our previous report.[37] The process is herein briefly described as follows. Firstly, 100 mg 11-MUA is added to 10 mL absolute ethanol to form a stock solution. Used as a catalyst, 100 μL H_2O is added to the stock solution. Thereafter, 10 mg AuNP–rGO, which has been pre-activated for 3 min under O_2 plasma, is immersed into the stock solution for about 8 h. Then the samples are sequentially filtrated and rinsed with ethanol and distilled water several times to remove the chemical residues. Finally, the material is dried under vacuum.

Loading sensing material onto microcantilever

A lab-made resonant microcantilever is used as the transducer for gas sensing. The cantilever has geometric dimensions of 200 μm length, 100 μm width and 3 μm thickness (detailed in ref. 34). Both the electrothermal resonance exciting and piezoresistive signal readout elements are integrated in the silicon cantilever. The cantilever features a high resonance *Q* factor that facilitates a high resolution of the frequency sensing signal. The 11-MUA functionalized AuNP–rGO sensing material (10 mg) is added into 1 mL distilled water (under ultrasonication) to form a crude suspension. Then, about 0.1 μL of the suspension is loaded onto the free end of the cantilever using a commercial micro-manipulator (Eppendorf, model PatchMan NP2). The loading process is controlled by the aid of inspection under a microscope (Leica, model DM4000). After drying in an oven at 45 °C for about 2 h, the microcantilever is ready for gas sensing. Although a constant volume of AuNP–rGO suspension is loaded using the commercial micro-manipulator, the loaded mass is generally slightly different among different cantilevers. We have fabricated and used quite a lot of cantilevers for the sensing experiments. Their resonant-frequency shifts due to the sensing-material loading are within a range of 15 kHz to 26 kHz. In order to ensure the consistency of the experimental results in this study, all of the experimental data relating to the functionalized AuNP–rGO are from the same cantilever sensor that exhibits the average sensing performance among the fabricated sensors. With the sensing material loaded onto the cantilever, the resonant frequency of the cantilever decreases from 100.675 kHz to 80.365 kHz. According to the designed mass-adsorption sensitivity of 1.53 Hz pg^{-1}, the mass of the loaded functionalized AuNP–rGO is estimated as about 13.3 ng.

Characterization

Raman measurements are performed in a Renishaw inVia system, where 100× objective and 532 nm wavelength laser light are used. X-ray diffraction (XRD) patterns are obtained by using a Bruker model D8 focus diffractometer equipped with a copper anode to produce X-rays (40 kV, 40 mA). The wavelength is 0.154 nm. The data are collected in a 5°–80° continuous scan mode. X-ray photoelectron spectroscopy (XPS) measurements are performed using a Thermo Scientific Escalab 250 system that is equipped with a monochromatic Al Kα X-ray source ($h\nu = 1486.6$ eV; spot size = 500 μm; power = 15 kV × 200 W). The curves of the obtained XPS spectra are fitted by data processing with the Avantage software. Nitrogen adsorption–desorption isotherms are measured at 77 K by using a Micromeritics ASAP 2020M system. The morphologies of the as-synthesized samples are characterized by using a transmission electron microscope (TEM, JEM-200CX) and a field-emission scanning electron microscope (FE-SEM, Hitachi S4800). Fourier transform infrared (FTIR) spectrum experiments are performed with a Bruker Vertex 70v FTIR spectrometer under vacuum (<100 Pa) using a KBr pellet. Contact-angle measurements are performed using a contact-angle measuring and contour analysis system (Dataphysics, OCA 15EC).

Gas sensing setup

We use a Pyrex glass testing chamber for the gas sensing experiments. Before detection, the microcantilever sensor is placed in the testing chamber for several minutes to obtain a stable baseline signal. Based on the pre-calculated concentration by volume dilution, a specific volume of the analyte gas is injected into the testing chamber. After detection, the testing chamber is switched to an open atmosphere, and the ultra-low concentration vapor can be rapidly swept away by air ventilation. For liquid analytes such as ethanol, however, we inject a constant volume of the liquid sample onto a small heating plate that is also placed in the testing chamber, to obtain homogenous vapor. The concentration can be estimated by the Clapeyron equation.[38]

Results and discussion

Characterization of the AuNP–rGO sensing material

The measured XRD patterns for the as-prepared graphite oxide, graphene oxide, AuNP–GO and AuNP–rGO are shown in Fig. 2a. The graphite oxide features a sharp peak at 9.6°. For the other three samples, however, the peak at 9.6° completely disappears and a broad peak centered at around 22.2° can be observed, which indicates a decreased interlayer distance. The AuNP–GO and AuNP–rGO samples have the same diffraction peaks at 2θ degrees of 38.2, 44.4, 64.5 and 77.5, which are assigned to face-centered cubic (fcc) Au (111), (200), (220) and (311), respectively. The XRD results are in agreement with the standard values of gold (JCPDS 04-0784).[39] Therefore, the XRD results confirm that AuNPs have been successfully grown *in situ* to form the AuNP–rGO nanostructure. The Raman spectra of the four samples are also shown in Fig. 2b for comparison. For the AuNP–rGO

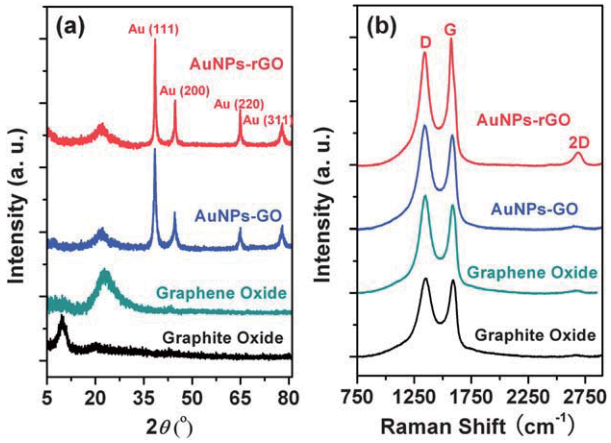

Fig. 2 XRD patterns (a) and Raman spectra (b) of graphite oxide, graphene oxide (GO), AuNP–GO and AuNP–rGO sheets.

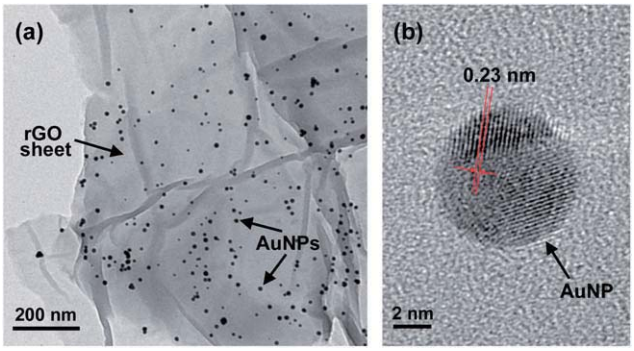

Fig. 4 (a) TEM image showing the as-prepared AuNP–rGO sheets. (b) HR-TEM image showing one AuNP grown *in situ* on the rGO sheet.

sample, there are three distinguishable peaks located at 1353 cm^{-1} (D peak), 1577 cm^{-1} (G peak) and 2711 cm^{-1} (2D peak). For the AuNP–GO sample, however, no obvious 2D peak is observed. Considering that the single 2D peak is one of the notable characteristics of rGO, thus the Raman characterization verifies that the AuNP–GO has been successfully reduced into AuNP–rGO by the gas-phase reducing reaction. This conclusion is also confirmed by XPS characterization. The C1s and O1s XPS spectra of the as-prepared AuNP–GO and AuNP–rGO sheets are shown in Fig. 3. After a Shirley background correction, the curve fitting for the C1s and O1s spectra is performed by using a Gaussian–Lorentzian peak shape. The peaks at 287.1 eV in C1s and 530.9 eV in O1s disappear in AuNP–rGO, which indicates the loss of oxygen during the reducing treatment in the Ar and H_2atmosphere. After reduction, the C/O atom ratio increases from 6.41 to 14.69, which further indicates the considerable deoxygenation by the reduction process.

The morphology of the as-prepared AuNP–rGO sample is observed by TEM. The TEM image in Fig. 4a verifies that the AuNPs have been successfully grown *in situ* on the rGO sheets. The HR-TEM image in Fig. 4b shows one AuNP with a 5 nm diameter and the crystal-lattice fringes that match (111)-Au. To verify that the rGO sheets are spaced by the AuNPs to form a porous-layered nano-stack structure, the porosity of the as-prepared AuNP–rGO sheets are measured using N_2 adsorption. As is shown in Fig. 5, the N_2 adsorption–desorption isotherms of the AuNP–rGO show a type II isotherm with the hysteresis type H3, which indicates the presence of mesopores and slit-shaped pores.[40] The sample features a BET specific surface-area of 120 m^2 g^{-1} and average mesopore size of 8.6 nm.

FTIR is used to characterize the 11-MUA functionalized AuNPs–rGO. As is shown in Fig. 6, the strong peak at around 3400 cm^{-1} is due to the stretching mode of –OH. The bands at 2927 cm^{-1} and 2849 cm^{-1} originate from the stretching of the $-CH_2$ groups. The distinguished peaks located at 1720 cm^{-1} and 1301 cm^{-1} can be assigned to the stretching modes of C=O and C–O groups, respectively, from the –COOH sensing group in the functionalized AuNP–rGO. The peak located at 1425 cm^{-1} can be ascribed to the carboxyl O=C–O or –OH bond.[41,42] The peak at 1630 cm^{-1} is due to the stretching mode of C=C in the aromatic rings of graphene. All of these characterizations confirm that the –COOH group has been successfully functionalized onto the prepared AuNP–rGO for the specific sensing of TMA molecules.

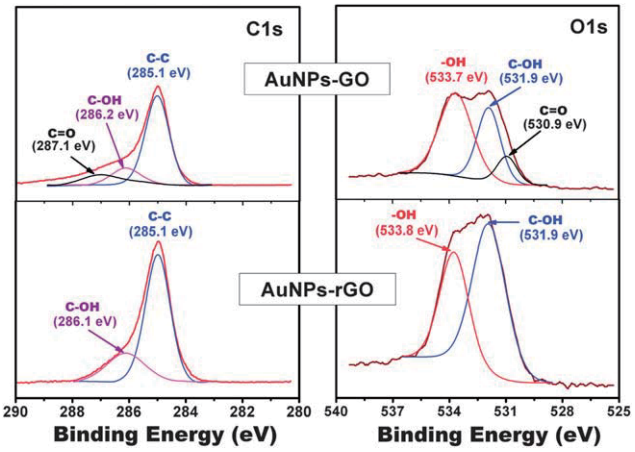

Fig. 3 C1s and O1s XPS spectra of AuNP–GO and AuNP–rGO.

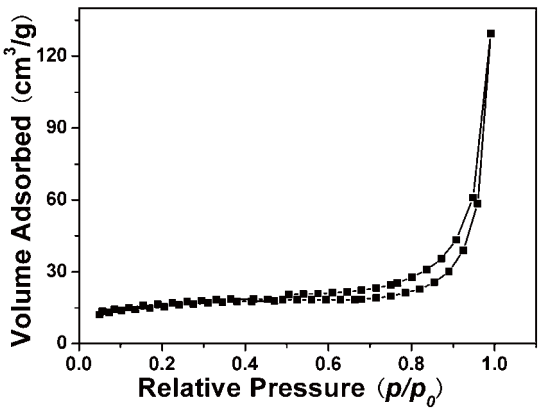

Fig. 5 N_2 adsorption–desorption isotherms of the porous-layered nano-stack structure formed by the AuNP–rGO sheets.

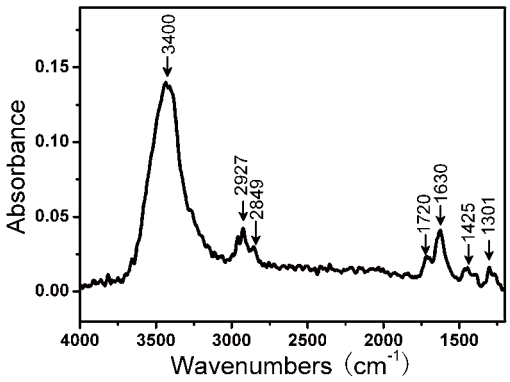

Fig. 6 FTIR spectrum of the AuNP–rGO sample that is functionalized with the sensing groups of 11-MUA.

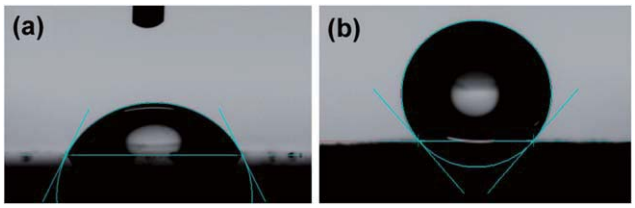

Fig. 7 Water-drop contact-angle (CA) measurements. (a) The surface of the AuNP–GO sheet shows hydrophilic properties (CA ≈ 61.6°). (b) The surface of the AuNP–rGO sheet shows hydrophobic properties (CA ≈ 131.5°).

The AuNP–rGO sheets feature a much stronger hydrophobicity than AuNP–GO because the quantity of oxygen-containing hydrophilic groups (*e.g.*, epoxide, carboxyl, and/or hydroxyl groups) in AuNP–rGO is much less than in AuNP–GO. This property is confirmed experimentally by the contact-angle (CA) measurements shown in Fig. 7. The water-drop CA on AuNP–rGO is about 131.5°, which is much larger than the CA of 61.6° on AuNP–GO. The high hydrophobicity of AuNP–rGO is very helpful in improving the sensing performance of the micro-gravimetric chemical sensors in terms of the depression of the humidity change-induced signal noise, since the highly hydrophobic AuNP–rGO can effectively suppress adsorption of moisture.

The SEM image in Fig. 8a shows the microcantilever which has the 11-MUA functionalized AuNP–rGO sensing material loaded near the free end. The magnified view of the porous-stacked nanostructure is shown in Fig. 8b, where the AuNPs spaced between the nanostructure layers can be clearly observed. As is shown in Fig. 8c, the presence of Au is proved by the energy dispersive spectroscopy (EDS) spectrum of the AuNP–rGO sheets.

Specific sensing to ppm-level TMA vapor

Equipped with a close-looped interface circuit, the microcantilever sensor is used to detect TMA vapor in real-time. After TMA vapor is injected into the testing chamber, the experimental results are recorded online and shown in Fig. 9a. With the concentration increasing stepwise in 5 ppm (parts per million) increments, the sensor outputs serial frequency-shift signals. The sensitivity of the sensor is obtained as about 3.5 Hz per

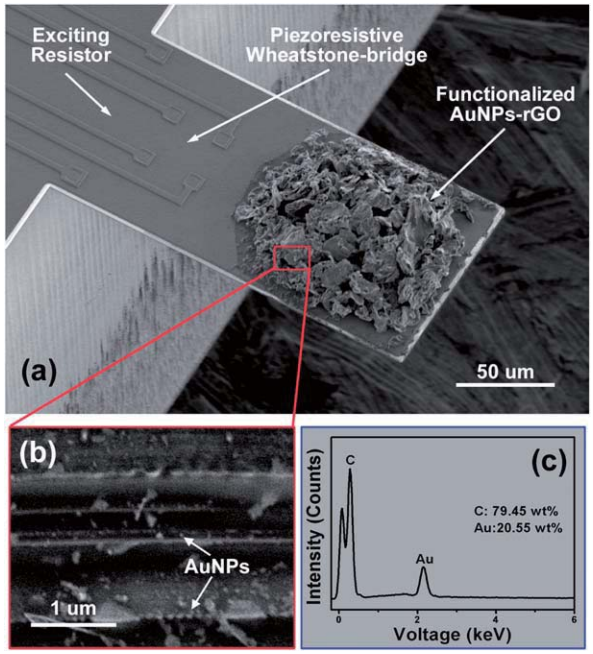

Fig. 8 (a) SEM image of the resonant microcantilever sensor with the AuNP–rGO sensing material coated at the free end. (b) Magnified view showing the AuNPs spaced between the nanostructure layers. (c) EDS spectrum for the porous-stacked AuNP–rGO sheets.

5 ppm, and there is no obvious attenuation in sensitivity during the multi-concentration continuing detection. Thanks to the porous-stacked nanostructure of the sensing material, the response of the sensor is very rapid, with the response time (t_{90}) being shorter than 30 s, where t_{90} is defined as the time period corresponding to the output signal amplitude reaching 90% of

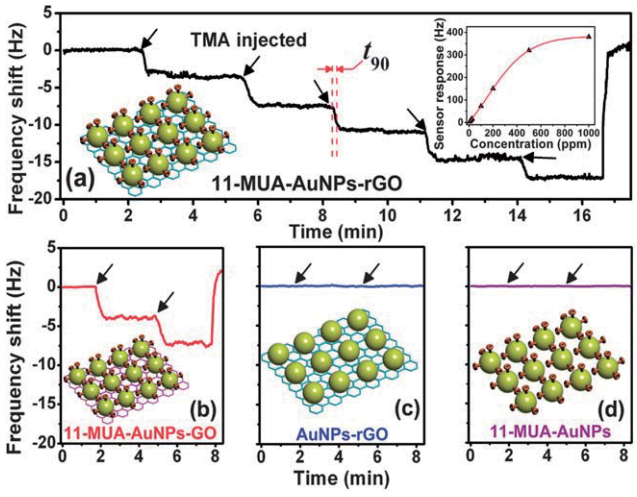

Fig. 9 Measured frequency sensing responses to trace TMA vapors. Identically designed microcantilevers are respectively loaded with different sensing materials: (a) 11-MUA functionalized AuNP–rGO; (b) 11-MUA functionalized AuNP–GO; (c) bare AuNP–rGO without functionalization; (d) 11-MUA functionalized colloidal AuNPs. The arrows denote the moments when the TMA vapor is sequentially injected into the testing chamber. The inset of Fig. 9a shows the sensing responses of the cantilever sensor loaded with 11-MUA functionalized AuNP–rGO *versus* the TMA vapor concentration from 5 ppm to 1000 ppm.

the maximal output value. After the multi-concentration detection, the sensor is carefully removed from the testing chamber and exposed to fresh air. Accordingly, the output signal of the sensor will recover to its original baseline, with the recovery time being shorter than 30 s.

Control experiments are also implemented, with the results shown in Fig. 9b–d. Compared with the sensor loaded with 11-MUA functionalized AuNP–rGO, the sensor loaded with the functionalized AuNP–GO exhibits a similar detection sensitivity to TMA (see Fig. 9b). Without functionalization, a similar amount of bare AuNP–rGO is loaded onto another identically structured microcantilever for TMA detection, resulting in no obvious response to 5 ppm TMA (see Fig. 9c). Without the rGO layers serving as the nano-stack shelves, colloidal AuNPs (5 nm particle size, purchased from Sigma-Aldrich) are also functionalized with 11-MUA and coated on a cantilever for TMA detection, also resulting in no obvious response signal.

The main superiority of the AuNP–rGO over the AuNP–GO lies in the depression of the noise from environmental humidity changes. To evaluate the capability to resist moisture adsorption, the cantilever loaded with the hydrophobic functionalized AuNP–rGO and another identically designed cantilever loaded with a similar amount of hydrophilic AuNP–GO are both used to detect humidity change, with the results shown in Fig. 10. Under a 100 ppm concentration change of H_2O vapor, the AuNP–rGO coated sensor has a response of 0.4 Hz that is much lower than the 2.8 Hz response of the AuNP–GO coated sensor.

Selectivity is one of the key parameters for chemical sensing. We choose ethanol (C_2H_5OH), carbon dioxide (CO_2), formaldehyde (HCHO), acetone (CH_3COCH_3) and benzene (C_6H_6) as interfering gases to investigate the selectivity of the sensing material, where all of the interfering gases have an identical concentration of 100 ppm. Using the two cantilever sensors (loaded with the 11-MUA functionalized AuNP–rGO and the 11-MUA functionalized AuNP–GO, respectively), we obtain the sensing responses to the interfering gases, humidity change and TMA, which are shown together in Fig. 11 for comparison. The cantilever sensor loaded with the 11-MUA functionalized AuNP–rGO always generates a response to the interfering gases of less than 3 Hz. Compared with the 7.1 Hz sensing response to the TMA vapor with a much lower concentration of 10 ppm, the satisfactory selectivity of the sensor is experimentally verified.

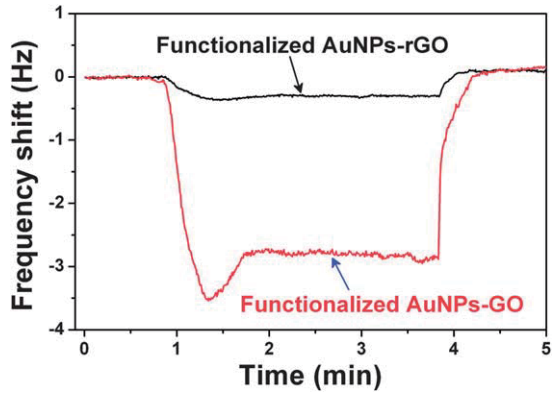

Fig. 10 Under the same humidity change (by vaporizing injected water in the detection chamber), the cantilever loaded with the functionalized AuNP–rGO sensing material shows a much lower response compared with another cantilever loaded with a similar amount of functionalized AuNP–GO.

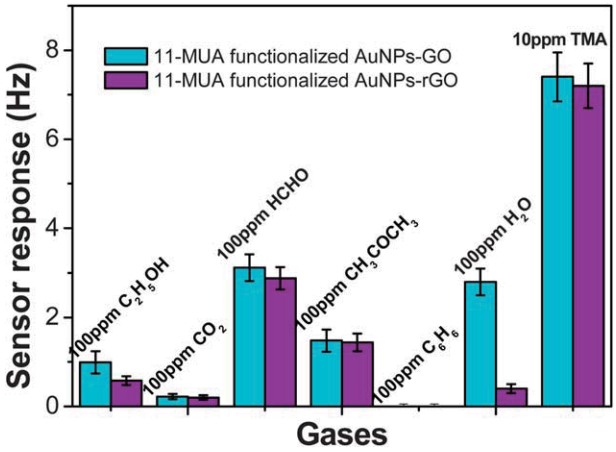

Fig. 11 Responses of the two sensors (used for obtaining the results in Fig. 10) to TMA of 10 ppm concentration and various interfering gases of 100 ppm concentration. The datum for each gas is averaged from three measurement results.

Conclusions

We have developed a simple method to construct a functionalized AuNP–rGO porously stacked nanostructure, which features a high effective specific surface area, as a sensing material for micro-gravimetric gas sensing. With 11-MUA sensing groups grafted onto the AuNPs, the novel sensing material is directly constructed onto the designated region of resonant microcantilevers. Sensing experiments and control tests are carried out, with the results verifying that the novel AuNP–rGO sensing material exhibits a rapid response, good selectivity and a high resolution to 5 ppm TMA vapor. Besides, thanks to the high hydrophobicity of the rGO sheets, the sensor exhibits a strong depression of the environmental noise from humidity changes. Such a novel sensing material is promising in various chemical vapor detection applications.

Acknowledgements

The work is supported by the Chinese 973 Program (2011CB309503), NSF of China (91023046, 61161120322, 61021064, 61102010) and the National Key Technology Support Program (2012BAK08B05). The Korean WCU project (R32-2009-000-20087-0) is acknowledged by Dong-Weon Lee and Xinxin Li.

Notes and references

1 P. van Rijn and A. Boker, *J. Mater. Chem.*, 2011, **21**, 16735.
2 M. C. Daniel and D. Astruc, *Chem. Rev.*, 2004, **104**, 293.
3 R. Elghanian, J. J. Storhoff, R. C. Mucic, R. L. Letsinger and C. A. Mirkin, *Science*, 1997, **277**, 1078.
4 Y. G. Sun and Y. N. Xia, *Science*, 2002, **298**, 2176.

5 U. H. F. Bunz and V. M. Rotello, *Angew. Chem., Int. Ed.*, 2010, **49**, 3268.
6 R. A. Sperling, P. Rivera gil, F. Zhang, M. Zanella and W. J. Parak, *Chem. Soc. Rev.*, 2008, **37**, 1896.
7 J. C. Love, L. A. Estroff, J. K. Kriebel, R. G. Nuzzo and G. M. Whitesides, *Chem. Rev.*, 2005, **105**, 1103.
8 E. Boisselier and D. Astruc, *Chem. Soc. Rev.*, 2009, **38**, 1759.
9 G. Zotti, B. Vercelli and A. Berlin, *Chem. Mater.*, 2008, **20**, 397.
10 H. Haick, *J. Phys. D: Appl. Phys.*, 2007, **40**, 7173.
11 M. Zayats, R. Baron, I. Popov and I. Willner, *Nano Lett.*, 2005, **5**, 21.
12 W. Z. Shen, M. Z. Li, B. L. Wang, J. Liu, Z. Y. Li, L. Jiang and Y. L. Song, *J. Mater. Chem.*, 2012, **22**, 8127.
13 K. Saha, S. S. Agasti, C. Kim, X. N. Li and V. M. Rotello, *Chem. Rev.*, 2012, **112**, 2739.
14 S. Y. Lin, C. H. Chen, M. C. Lin and H. F. Hsu, *Anal. Chem.*, 2005, **77**, 4821.
15 S. O. Obare, R. E. Hollowell and C. J. Murphy, *Langmuir*, 2002, **18**, 10407.
16 A. J. Reynolds, A. H. Haines and D. A. Russell, *Langmuir*, 2006, **22**, 1156.
17 B. I. Ipe, K. Yoosaf and K. G. Thomas, *J. Am. Chem. Soc.*, 2006, **128**, 1907.
18 Y. He and H. Cui, *J. Mater. Chem.*, 2012, **22**, 9086.
19 L. Dyadyusha, H. Yin, S. Jaiswal, T. Brown, J. J. Baumberg, F. P. Booy and T. Melvin, *Chem. Commun.*, 2005, 3201.
20 Y. Xiao, F. Patolsky, E. Katz, J. F. Hainfeld and I. Willner, *Science*, 2003, **299**, 1877.
21 M. Zayats, E. Katz, R. Baron and I. Willner, *J. Am. Chem. Soc.*, 2005, **127**, 12400.
22 X. X. Li and D. W. Lee, *Meas. Sci. Technol.*, 2012, **23**, 022001.
23 Y. J. Liu, P. C. Xu, H. T. Yu, G. M. Zuo, Z. X. Cheng, D.-W. Lee and X. X. Li, *J. Mater. Chem.*, 2012, **22**, 18004.
24 P. C. Xu, H. T. Yu and X. X. Li, *Anal. Chem.*, 2011, **83**, 3448.
25 H. T. Yu, P. C. Xu, X. Y. Xia, D. W. Lee and X. X. Li, *IEEE Trans. Ind. Electron.*, 2012, **59**, 4881.
26 H. T. Yu, T. T. Yang, Y. Chen, P. C. Xu, D. W. Lee and X. X. Li, *Anal. Chem.*, 2012, **84**, 6679.
27 J. W. Grate, D. A. Nelson and R. Skaggs, *Anal. Chem.*, 2003, **75**, 1868.
28 J. W. Grate, *Anal. Chem.*, 2003, **75**, 6759.
29 R. Hao, W. Qian, L. H. Zhang and Y. L. Hou, *Chem. Commun.*, 2008, 6576.
30 M. J. Allen, V. C. Tung and R. B. Kaner, *Chem. Rev.*, 2010, **110**, 132.
31 X. Cui, C. Z. Zhang, R. Hao and Y. L. Hou, *Nanoscale*, 2011, **3**, 2118.
32 C. Z. Zhang, R. Hao, H. B. Liao and Y. L. Hou, *Nano Energy*, 2013, **2**, 88.
33 C. Z. Zhang, R. Hao, H. Yin, F. Liu and Y. L. Hou, *Nanoscale*, 2012, **4**, 7326.
34 H. T. Yu, X. X. Li, X. H. Gan, Y. J. Liu, X. Liu, P. C. Xu, J. G. Li and M. Liu, *J. Micromech. Microeng.*, 2009, **19**, 045023.
35 X. M. Sun, Z. Liu, K. Welsher, J. T. Robinson, A. Goodwin, S. Zaric and H. J. Dai, *Nano Res.*, 2008, **1**, 203.
36 X. F. Zhou and Z. P. Liu, *Chem. Commun.*, 2010, **46**, 2611.
37 G. M. Zuo, X. X. Li, P. Li, T. T. Yang, Y. L. Wang, Z. X. Cheng and S. L. Feng, *Anal. Chim. Acta*, 2006, **580**, 123.
38 P. Saurel, *J. Phys. Chem. C*, 1901, **5**, 256.
39 H. Zhang, J. J. Xu and H. Y. Chen, *J. Phys. Chem. C*, 2008, **112**, 13886.
40 M. Kruk and M. Jaroniec, *Chem. Mater.*, 2001, **13**, 3169.
41 S. Y. Wang, D. S. Yu, L. M. Dai, D. W. Chang and J.-B. Baek, *ACS Nano*, 2011, **5**, 6202.
42 R. L. Shriner, C. K. F. Hermann, T. C. Morrill, D. Y. Curtin and R. C. Fuson, in *The Systematic Identification of Organic Compounds*, Wiley, 8th edn, 2004.

